Coupled Systems Mechanics, *Vol. 13, No. 5 (2024) 375-393*
https://doi.org/10.12989/csm.2024.13.5.375

A nonlocal strain gradient model for buckling analysis of advanced FG CNT-reinforced composite nanobeams

Djillali Mokhefi[1], Aicha Bessaim[1], Mohammed Sid Ahmed Houari*[1], Zakaria Deffane[2], Hakima Houari-Belkadi[3], Belhocine Ali[1], Ahmed Amine Daikh[1,4], Habib Hebali[1], Hadj Youzera[1] and Tarek Merzouki[6]

[1]*Laboratoire d'Etude des Structures et de Mécanique des Matériaux, Département de Génie Civil, Faculté des Sciences et de la Technologie, Université Mustapha Stambouli, B.P. 305, R.P., Mascara 29000, Algeria*
[2]*Aerospace Engineering Division, Universitat Politécnica de Catalunya, 08034, Barcelona, Spain*
[3]*Dental Technology and Biomaterials Research Laboratory, Department of Dentistry-Oran's, Faculty of Medicine, University of Oran, 31000, Algeria*
[4]*Artificial Intelligence Laboratory for Mechanical and Civil Structures, and Soil, University Centre of Naama, P.O. Box 66, Naama 45000, Algeria*
[5]*LISV, University of Versailles Saint-Quentin, 10-12 avenue de l'Europe, 78140 Vélizy, France*

(Received May 2, 2024, Revised July 26, 2024, Accepted August 7, 2024)

Abstract. The main objective of this paper is to investigate the buckling behavior of symmetric and non-symmetric carbon nanotube-reinforced composite (CNTRC) nanobeams with nonlocal strain gradient effects. For this purpose, a novel trigonometric shear deformation beam theory is employed, and the Galerkin method is used for analysis. The carbon nanotube-reinforced composite beam consists of a polymeric matrix reinforced with aligned and distributed single-walled carbon nanotubes (SWCNTs) having various reinforcement patterns. The material properties of the carbon nanotube-reinforced composite beams are estimated using the rule of mixture. The governing equations of the problem are derived based on the principle of total potential energy. The proposed theory accurately represents the parabolic distribution of transverse shear stress across the beam thickness and satisfies the zero traction boundary conditions on the top and bottom surfaces without requiring shear correction factors. The mathematical models presented in this work are validated numerically by comparing them with existing literature to assess their accuracy and reliability. The buckling analyses of the carbon nanotube-reinforced composite nanobeams are conducted, considering various factors such as beam types, nonlocal length-scale parameter, strain gradient microstructure-scale parameter, geometry, carbon nanotube volume fraction, and boundary conditions. Additionally, new results are reported in this study, which can serve as a benchmark for future research.

Keywords: CNTRC beams; elastic buckling; Galerkin method; higher order nonlocal strain gradient theory; shear deformation beam theory

1. Introduction

*Corresponding author, Professor, E-mail: ms.houari@univ-mascara.dz

http://www.techno-press.org/?journal=csm&subpage=8 ISSN: 2234-2184 (Print), 2234-2192 (Online)

Since their discovery, carbon nanotubes (CNTs) have been widely recognized for their exceptional qualities, which include high elastic modulus, tensile strength, low density, extraordinary strength and corrosion resistance, and high-performance structural and multifunctional composites (Wattanasakulpong and Ungbhakorn 2013, De Borbón *et al.* 2014, Daikh *et al.* 2020a, Alazwari *et al.* 2021). The initial idea of carbon nanotubes (CNTs) as a type of novel material with excellent properties was proposed by Iijima (1991). One of the significant applications of CNTs is to design nanosensors owing to their exceptional mechanical properties, which leads to a reachable ultra-high frequency range up to the terahertz order and a possible ultrahigh sensitivity. Carbon nanotubes that can provide good interfacial bonds have been utilized instead of traditional fibres to reinforce matrix phases in polymer composites. By convention, polymer composites reinforced by carbon, aramid, glass or basalt fibres have vast applications in structural designs in civil, mechanical, marine, aerospace structural composites and considerably other modern industries (Yamamoto *et al.* 2012). The fundamental challenge of producing carbon nanotube composites (CNTRCs) is enhancing the dispersion and alignment of CNTs in a polymer matrix. However, shortcomings are also present. Firstly, this sort of fiber-reinforced composite is often manufactured as laminated composites with variable fiber orientations at different layers, and mismatching material qualities can result in delamination. Secondly, debonding or microscopic defects between fibres and matrix are prevalent because of their relatively high volume fraction of fillers. As a consequence, the overall performance of structural elements is degraded (Okamoto, 2006).

Composites reinforced by nanoscale fillers have emerged as an option for the new generations of advanced composite materials due to the rapid advancement of developed nanomaterial technology. Unlike their micron-scale equivalents, the physical characteristics of nanocomposites can be changed at extremely low nanofiller weight percentages. While the interface zones between nanoparticles and matrix are remarkably more significant for a given volume percentage (Lin *et al.* 2014). One incorporated into the matrix, aligned CNT array, thin films or wires not only enhance the mechanical properties along the alignment direction but also affect the thermal and electrical conductivity of nanocomposites at a specific direction. Shen (2009) incorporated functionally graded materials (FGM) into the nanocomposites by varying the volume fraction of aligned CNTs along the thickness direction of plates. Who can foresee that the final structural element will have unique properties that can tailor in terms of vibration control, durability, and electrical and thermal conductivities. Several experimental and theoretical methods, such as rule of mixing (Alibeigloo 2014, Lin and Xiang, 2014, Shen and Xiang, 2012), representative volume element (RVE), and experiments (King *et al.* 2012, Salem *et al.* 2015, Sagar *et al.* 2015), have been provided to investigate the mechanical behavior of CNT-reinforced composites and simulate their effective material characteristics. In the current vicennial, many demands have been raised for the production of multilayer micro- and nanoelectromechanical systems (MEMS and NEMS) with variable properties which are used in the thermal environment (Witvrouw and Mehta 2005). Consequently, several studies have concentrated on the thermal (Daikh *et al.* 2021, Zhao *et al.* 2022) and mechanical (Daikh *et al.* 2022, Khadir *et al.* 2021, Bachiri *et al.* 2022, Gia Phi *et al.* 2022, Drai *et al.* 2023, Gholami *et al.* 2023, Tlidji *et al.* 2022, Alazwari *et al.* 2022, Eyvazian *et al.* 2021, Ghandourah *et al.* 2021, Zhao *et al.* 2022, Khadir *et al.* 2021, Esmaeilzadeh *et al.* 2021, Bouafia *et al.* 2021, Gholami *et al.* 2023, Drai *et al.* 2023) properties of FG micro- and nanostructures. By employing the Euler–Bernoulli beam theory and von Kármán geometric nonlinearity, Rafiee *et al.* (2013) studied the non-linear free vibration of carbon nanotube-reinforced composite beams with a piezoelectric layer on the surface subjected to a combined

effect of heat and electric charge. Based on first-order shear deformation theory (FSDT), Ke *et al.* (2013) investigated the dynamic instability of a single-layer FG-CNTRC beam. They evaluated the material properties of the FG-CNTRC beam using an extended mixture rule.

Daikh *et al.* (2022) studied the mechanical responses of a simply supported multilayer nanobeam reinforced by CNTs under various loading profiles using a novel hyperbolic shear deformation beam theory and non-local strain gradient theory. Zhao *et al.* (2022) implemented first order shear deformation theory in analyzing the vibration characteristics of FG carbon nanotube-reinforced composite double-beams in thermal environments. Chen *et al.* (2021) studied the vibration analysis of functionally graded carbon nanotube reinforced fluid-conveying tube in thermal environment. Dang *et al.* (2022) introduced a model of a functionally graded (FG) nanotube conveying fluid embedded in an elastic medium based on the nonlocal strain gradient theory in conjunction with Euler-Bernoulli beam theory. Shen and Yang (2013) used higher-order shear deformation theory to analyze free vibrations, nonlinear bending, and post-buckling beams made of FG-CNTRC reinforced composites on an elastic foundation. Gia *et al.* (2022) have revealed the nonlinear free vibration behavior of reinforced microbeams with piezoelectric layers. Wu *et al.* (2017) used the FSDT to study the thermal post-buckling of temperature-dependent FG-CNTRC beams with various geometric imperfections. Yas and Samadi (2012) investigated the free vibrations and buckling of FG-CNTRC Timoshenko beams using the extended differential quadrature method (DQM). As far as authors are aware, there is currently no publication available that explains the buckling behaviors of FG-CNTRC nanobeams under various boundary conditions using an analytical solution based on the new shear deformation theory and nonlocal strain gradient theory.

Recent advancements in multi-scale modeling have significantly enhanced our understanding of material behavior under various conditions. Moreno-Navarro *et al.* (2021) developed a 3D lattice-type model capturing the nonlinear coupling between mechanical and electric fields, integrating ferroelectric behavior and plasticity with kinematic hardening. Suljevic *et al.* (2022) tackled parameter identification for 3D concrete plasticity models using a multi-scale framework, achieving computational efficiency through a staged identification process. Ibrahimbegovic and Nava (2021) introduced a damping model within a multi-scale analysis framework to predict vibration amplitude reduction, adaptable to any structure size and frequency range. Hajdo *et al.* (2021) explored instability of frame structures under nonconservative loads using dynamic finite element models, validated against analytical solutions. Ibrahimbegovic *et al.* (2022) compared deterministic and stochastic approaches to beam instability, using a reduced model and stochastic framework to account for material heterogeneities, offering robust solutions for complex engineering problems.

The main contribution of the current study is to develop size-dependent exact solutions buckling of FG-carbon nanotube-reinforced composite nanobeams in the framework of nonlocal strain gradient elasticity theory. Material properties of FG-CNTRCs are assumed to be graded in the thickness direction and computed via the extended mixture rule. The governing equations of the problem are derived based on the principle of total potential energy. The proposed theory accurately represents the parabolic distribution of transverse shear stress across the beam thickness and satisfies the zero traction boundary conditions on the top and bottom surfaces without requiring shear correction factors. The mathematical models presented in this work are validated numerically by comparing them with existing literature to assess their accuracy and reliability. The buckling analyses of CNTRC nanobeams are conducted, considering various factors such as beam types, nonlocal length-scale parameter, strain gradient microstructure-scale parameter, geometry,

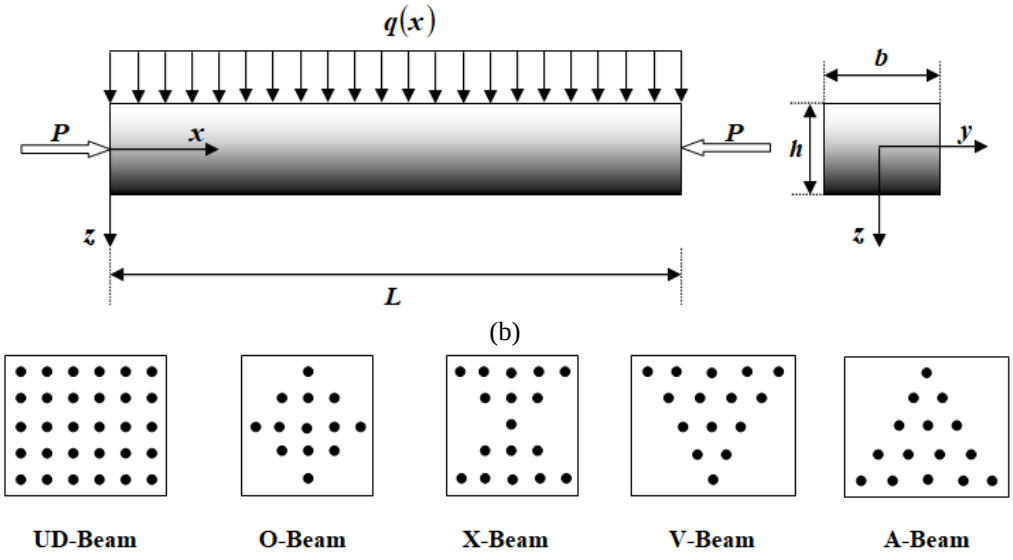

Fig. 1 Configuration, loading and coordinate system of a CNTRC beam (a) and cross sections of different patterns of reinforcement (b)

carbon nanotube volume fraction, and boundary conditions. Additionally, new results are reported in this study, which can serve as a benchmark for future research.

2. Mathematical formulation

Consider a uniform carbon nanotube-reinforced composites beam of thickness h, length L, and width b made by mixing two distinct materials (SWCNT and an isotropic polymer matrix).

The coordinate system for carbon nanotube-reinforced composite beam is shown in Fig. 1(a). The beams are assumed to have five distinct reinforcement patterns over the cross sections, as shown in Fig. 1(b).

Using the rule of mixture, the effective material properties of CNTRC beams can be estimated. The effective material properties of the carbon nanotube-reinforced composite beams can be estimated using the rule of mixture.

The expressions of the effective Young's of the carbon nanotube-reinforced composite beam modulus and shear modulus are therefore as follows (Wattanasakulpong and Ungbhakorn 2013)

$$\begin{aligned} E_{11} &= \eta_1 V_{cnt} E_{11}^{cnt} + V_p E^p \\ \frac{\eta_2}{E_{22}} &= \frac{V_{cnt}}{E_{22}^{cnt}} + \frac{V_p}{E^p} \\ \frac{\eta_3}{G_{12}} &= \frac{V_{cnt}}{G_{12}^{cnt}} + \frac{V_p}{G^p} \end{aligned} \tag{1}$$

Here, E_{11}, E_{22} and G_{12} are Young's moduli in x-direction, Young's moduli in z-direction, and the shear modulus of the CNTRC beam, respectively, where superscriptsp and cnt refer to the

Table 1 The CNTs efficiency parameters

V_{cnt}^{*}	η_1	η_2	η_3
0.12	1.2833	1.0556	1.0556
0.17	1.3414	1.7101	1.7101
0.28	1.3238	1.7380	1.7380

properties of the matrix and the CNTs. Also, V_{cnt} and V_p are the volume fractions for carbon nanotube and the polymer matrix, respectively, with the relation of $V_{cnt} + V_p = 1$.

The CNT performance parameters $\eta_i (i = 1,2,3)$ are introduced to consider the size-dependent material properties of SWCNT. They can be calculated by comparing the carbon nanotube-reinforced composite elastic modules estimated by the MD simulation to the numerical results estimated by the mixture rule (Wattanasakulpong and Ungbhakorn 2013). By applying the same law, Poisson's ratio (ν) and mass density (ρ) of the CNTRC beams are written as

$$\nu = V_{cnt}\nu^{cnt} + V_p\nu^p, \ \rho = V_{cnt}\rho^{cnt} + V_p\rho^p \tag{2}$$

where ν^{cnt}, ν^p and ρ^{cnt}, ρ^p are the Poisson's ratios and densities of the CNT and polymer matrix respectively. For different patterns of carbon nanotube reinforcement distributed across the cross sections of the beams as shown in Fig. 1(b), the continuous mathematical functions used to describe the material component distributions are given below: The CNT volume fractions V_{cnt} of various types of the FG-CNTRC beam as shown in Fig. 1(b) can be expressed as

$$V_{cnt} = \begin{cases} V_{cnt}^{*} & \text{UD CNTRC} \\ 4\frac{|z|}{h}V_{cnt}^{*} & \text{FG-X CNTRC} \\ 2\left(1 - \frac{2|z|}{h}\right)V_{cnt}^{*} & \text{FG-O CNTRC} \\ \left(1 - \frac{2z}{h}\right)V_{cnt}^{*} & \text{FG-V CNTRC} \end{cases} \tag{3}$$

where FG-V CNTRC, FG-O CNTRC and FG-X CNTRC indicate the non-uniform functionally graded distributions, and UD CNTRC indicate the uniform distribution $\mathrm{V_{cnt}^{*}}$ is the total volume fraction of CNTs, which can be calculate from the following equation (Yas and Samadi 2012)

$$V_{cnt}^{*} = \frac{W_{cnt}}{W_{cnt} + (\rho^{cnt}/\rho^{m})(1 - W_{cnt})} \tag{4}$$

where $\mathrm{V_{cnt}^{*}}$, $\mathrm{\rho^{cnt}}$ and ρ^m are the CNTs mass fraction, CNTs mass density and polymer matrix mass density, respectively.

In this study, the CNT efficiency parameters η_i associated with the given volume fraction V_{cnt}^{*} are (Table1).

The parameters $\mathrm{\eta_i}(i = 1,2,3)$ are the CNTs efficiency parameters.

3. Nonlocal strain gradient theory

The nonlocal strain gradient theories are based on size dependent continuum mechanics that accounts for small scale effects in constitutive equations. When dealing with nano-structures, the effect of size dependent can't be ignored in the process of analysis. Nonlocal strain gradient

elasticity proposed by Lim *et al.* (2015) gives the expression of the total stress tensor as a function of the standard nonlocal stress tensor and the strain gradient stress tensor

$$\sigma_{ij} = \sigma_{ij}^{(0)} - \frac{\partial \sigma_{ij}^{(1)}}{\partial x} \tag{5}$$

Where the stress $\sigma_{ij}^{(0)}$ corresponds to the strain ε_{kl} and the higher order stress $\sigma_{ij}^{(1)}$ corresponds to the gradient of the strain $\varepsilon_{kl,x}$ and are defined by

$$\sigma_{ij}^{(0)} = \int_0^L C_{ijkl}\alpha_0(x, x', e_0 a)\varepsilon'_{kl}(x')dx' \tag{6a}$$

$$\sigma_{ij}^{(1)} = l^2 \int_0^L C_{ijkl}\alpha_1(x, x', e_1 a)\varepsilon_{kl,x}(x')dx' \tag{6b}$$

In which C_{ijkl} are the elastic constants and $e_0 a$ and $e_1 a$ consider the influences of the non-local stress field, and l indicates the length scale parameter of the material and captures the stress field effects of the strain gradient of higher order. When the nonlocal functions fulfill the conditions developed by Eringen (1972, 1983), the constitutive relation for an nanobeams can be stated as

$$(1-(e_1 a)^2\nabla^2)\ (1-(e_0 a)^2\nabla^2)\ \sigma_{ij} = C_{ijkl}(1-(e_1 a)^2\nabla^2)\ \varepsilon_{kl} - C_{ijkl}(1-(e_0 a)^2\nabla^2)\ \nabla^2\varepsilon_{kl} \tag{6c}$$

In which ∇^2 indicates the Laplacian operator. Supposing $e_1 = e_0 = e$ and by eliminating the order terms $O\nabla^2$, the general constitutive relation in Eq. (27) can be rewritten as (Eringen 1972, Eringen 1983)

$$(1-(ea)^2\nabla^2)\ \sigma_{ij} = C_{ijkl}(1-(l)^2\nabla^2)\ \varepsilon_{kl} \tag{7}$$

where $\mu = (ea)^2$ and $\lambda = l^2$

By elsewhere, the relationships constituent for a CNTRC deformable in shear nanobeam room sandwich can be writing as

$$\begin{aligned} \sigma_{xx} - \mu\frac{\partial^2\sigma_{xx}}{\partial x^2} &= C_{11}\left(\varepsilon_{xx} - \lambda\frac{\partial^2\varepsilon_{xx}}{\partial x^2}\right) \\ \sigma_{xz} - \mu\frac{\partial^2\sigma_{xz}}{\partial x^2} &= C_{55}\left(\gamma_{xz} - \lambda\frac{\partial^2\gamma_{xz}}{\partial x^2}\right) \end{aligned} \tag{8}$$

It is of interest that Eq. (8) can be simplified to some interested cases.

3.1 Nonlocal elasticity theory

The constitutive equation of the nonlocal elasticity theory can be easily obtained by setting $\lambda = 0$ in the nonlocal strain gradient constitutive Eq. (8) as

$$\begin{aligned} \sigma_{xx} - \mu\frac{\partial^2\sigma_{xx}}{\partial x^2} &= C_{11}\varepsilon_{xx} \\ \sigma_{xz} - \mu\frac{\partial^2\sigma_{xz}}{\partial x^2} &= C_{55}\gamma_{xz} \end{aligned} \tag{9}$$

which are identical to Eringen (1972b), Eringen and Edelen (1972), Eringen (1983b).

3.2 Strain gradient theory

The constitutive equation of the strain gradient theory can be easily obtained by setting $\mu = 0$ in Eq. (12), that is

$$\begin{aligned} \sigma_{xx} &= C_{11}\left(\varepsilon_{xx} - \lambda\frac{\partial^2\varepsilon_{xx}}{\partial x^2}\right) \\ \sigma_{xz} &= C_{55}\left(\gamma_{xz} - \lambda\frac{\partial^2\gamma_{xz}}{\partial x^2}\right) \end{aligned} \tag{10}$$

which are identical to Aifantis and Willis (2005), Aifantis (1992). It is shown that, the general constitutive Eq. (12) can reasonably explain size-dependent phenomena and there is a good agreement between the molecular dynamics simulations and the nonlocal strain gradient theory Lim *et al.* (2015), Li *et al.* (2016).

4. Governing equation for size-dependent nanobeams

A quasi-2D parabolic shear deformation beam theory for of CNTRC nanobeam considering transverse shear deformations is adopted in this study. The displacement field of the proposed theory is chosen based on the following assumptions:

(1) The axial displacement consists of extension, bending and shear components,

(2) The bending component of axial displacement is similar to that given by the Euler–Bernoulli beam theory,

(3) The shear component of axial displacement gives rise to the parabolic variation of shear strain and hence to shear stress through the thickness of the beam in such a way that shear stress vanishes on the top and bottom surfaces.

4.1 Kinematics

Based on the assumptions made above, the displacement field of the present theory can be obtained as

$$\begin{aligned} u(x,z) &= u_0(x) - z\frac{\partial w}{\partial x} + f(z)\phi_x(x) \\ w(x) &= w_0(x) \end{aligned} \tag{11}$$

where $u_0(x)$ is the axial displacement, $w_0(x)$ is the transverse displacement of a mid-line point of the beam, $\phi_x(x)$ is the rotation of a cross section of the beam at the neutral axis due to transverse shear deformation.

The hyperbolic function that illustrates the shear deformation along with thickness direction is shown through the next stage

$$f(z) = z\left(\frac{\pi + 2\,cos(\pi z/h)}{\pi + 2}\right) \tag{12}$$

The kinematic strain components associated with the displacements are stated as

$$\begin{aligned}\varepsilon_{xx} &= \varepsilon_{xx}^{(0)} + z\varepsilon_{xx}^{(1)} + f(z)\varepsilon_{xx}^{(2)} \\ \gamma_{xz} &= g(z)\gamma_{xz}^{(0)}\end{aligned} \tag{13}$$

where

$$\varepsilon_{xx}^{(0)} = \frac{\partial u_0}{\partial x},\ \varepsilon_{xx}^{(1)} = \frac{\partial^2 w_0}{\partial x^2},\ \varepsilon_{xx}^{(2)} = \frac{\partial \phi_x}{\partial x},\ \gamma_{xz}^{(0)} = \phi_x \tag{14a}$$

The function $g(z)$is given as follows

$$g(z) = f'(z) \tag{14b}$$

4.2 Variational statements

The governing equations of motion in terms of displacements are derived using Hamilton's Principle. The dynamic version of the principle of virtual displacement takes the following form (Belarbi *et al.* 2022)

$$\int_{t_1}^{t_2} (\delta U + \delta V - \delta K)dt = 0 \tag{15}$$

where t is the time, t_1 and t_2 are the initial and end time, respectively, $\delta\ U$ is the virtual variation of the strain energy, $\delta\ V$ is the variation of work done by external forces, and $\delta\ K$ is the virtual variation of the kinetic energy.

The variation of the strain energy of the beam can be stated as

$$\begin{aligned}\delta U &= \int_0^L \int_{-h/2}^{h/2} \left(\sigma_{xx}^{(0)}\delta\varepsilon_{xx} + \sigma_{xz}^{(0)}\delta\gamma_{xz} + \sigma_{xx}^{(1)}\nabla\delta\varepsilon_{xx} + \sigma_{xz}^{(1)}\nabla\delta\gamma_{xz}\right) dz\, dx \\ &= \int_0^L \int_{-h/2}^{h/2} \left(\left(\sigma_{xx}^{(0)} - \nabla\sigma_{xx}^{(1)}\right)\delta\varepsilon_{xx} + \left(\sigma_{xz}^{(0)} - \nabla\sigma_{xz}^{(1)}\right)\delta\gamma_{xz}\right) dz\, dx + \left[\int_0^L \int_{-h/2}^{h/2} \left(\sigma_{xx}^{(1)}\nabla\delta\varepsilon_{xx} + \sigma_{xz}^{(1)}\nabla\delta\gamma_{xz}\right) dz dx\right]_0^L \\ &= \int_0^L \int_{-h/2}^{h/2} (\sigma_{xx}\delta\varepsilon_{xx} + \sigma_{xz}\delta\gamma_{xz})\, dz\, dx + \left[\int_0^L \int_{-h/2}^{h/2} \left(\sigma_{xx}^{(1)}\delta\varepsilon_{xx} + \sigma_{xz}^{(1)}\delta\gamma_{xz}\right) dz dx\right]_0^L\end{aligned} \tag{16}$$

Here, force and moment fields are defined from the stress components as follow

$$[N_x, M_x, S_x] = \int_{-h/2}^{h/2} [1, z, f(z)]\ \sigma_x dz\,,\ Q_{xz} = \int_{-h/2}^{h/2} g(z)\tau_{xz} dz \tag{17a}$$

$$\left[N_x^{(1)}, M_x^{(1)}, S_x^{(1)}\right] = \int_{-h/2}^{h/2} [1, z, f(z)]\ \sigma_x^{(1)} dz\,,\ Q_{xz}^{(1)} = \int_{-h/2}^{h/2} g(z)\tau_{xz}^{(1)} dz \tag{17b}$$

Thus, the virtual strain energy can be rewritten as

$$\begin{aligned}\delta U = &\int_0^L \left(N_x \frac{\partial \delta u_0}{\partial x} - M_x \frac{\partial^2 \delta w_0}{\partial x^2} + S_x \frac{\partial \delta \phi_x}{\partial x} + Q_{xz}\delta\phi_x\right) dx \\ &+ \left[N_x^{(1)} \frac{\partial \delta u_0}{\partial x} - M_x^{(1)} \frac{\partial^2 \delta w_0}{\partial x^2} + S_x^{(1)} \frac{\partial \delta \phi_x}{\partial x} + Q_{xz}^{(1)}\delta\phi_x\right]_0^L\end{aligned} \tag{18}$$

Following the same approach for the variation of the kinetic energy, we obtain as

$$\begin{aligned}\delta K &= \int_0^L \int_{-\frac{h}{2}}^{\frac{h}{2}} \rho(z)[\dot{u}\delta\dot{u} + \dot{w}\delta\dot{w}]\, dzdx \\ &= \int_0^L \int_{-h/2}^{h/2} \rho(z)\left[\left(\dot{u}_0 - z\frac{\partial \dot{w}_0}{\partial x} + \Psi(z)\dot{\phi}_x\right)\left(\delta\dot{u}_0 - z\frac{\partial \delta\dot{w}_0}{\partial x} + \Psi(z)\delta\dot{\phi}_x\right) + \dot{w}_0\ \delta\dot{w}_0\right] dzdx = \\ &\int_0^L \left\{\left(I_0\dot{u}_0 - I_1\frac{\partial \dot{w}_0}{\partial x} + J_1\dot{\phi}_x\right)\delta\dot{u}_0\right. \\ &\left. + \left((I_0\dot{w}_0)\delta\dot{w}_0 - \left(I_1\dot{u}_0 - I_2\frac{\partial \dot{w}_0}{\partial x} + J_2\dot{\phi}_x\right)\frac{\partial \delta\dot{w}_0}{\partial x}\right) + \left(J_1\dot{u}_0 - J_2\frac{\partial \dot{w}_0}{\partial x} + K_2\dot{\phi}_x\right)\delta\dot{\phi}_x\right\} dx\end{aligned} \tag{19}$$

where the dot-exponent convention indicates the differentiation with respect to the time variable t, and (I_i, J_i, K_i) are mass inertias defined as

$$(I_0, I_1, I_2, J_0, J_1, J_2, K_2) = \int_{-\frac{h}{2}}^{\frac{h}{2}} (1, z, z^2, \Psi', \Psi, z\,\Psi, \Psi^2)\rho(z)dz \tag{20}$$

The first variation of the work done by the distributed external forces q acting on the upper surface ($z = h/2$) in the normal direction and the axial compressive force is given by

$$\delta V = \int_0^L q\delta w_0 dx + \int_0^L N_0 \frac{\partial w_0}{\partial x}\frac{\partial \delta w_0}{\partial x}\delta w dx \tag{21}$$

The following governing equations are derived from the variation principle Eq. (14) by introducing Eqs. (18), (19), (21), and proceeding to some integrations by parts

$$\begin{aligned}\delta u_0 &: \frac{\partial N_x}{\partial x} = I_0\ddot{u}_0 - I_1\frac{\partial \ddot{w}_0}{\partial x} + J_1\ddot{\phi}_x \\ \delta w_0 &: \frac{\partial^2 M_x}{\partial x^2} + q - N_0\frac{\partial^2 w_0}{\partial x^2} = -I_1\frac{\partial \ddot{u}_0}{\partial x} + I_0\ddot{w}_0 + I_2\frac{\partial^2 \ddot{w}_0}{\partial x^2} - J_2\frac{\partial \ddot{\phi}_x}{\partial x} \\ \delta\phi_x &: \frac{\partial S_x}{\partial x} - Q_{xz} = J_1\ddot{u}_0 - J_2\frac{\partial \ddot{w}_0}{\partial x} + K_2\ddot{\phi}_x\end{aligned} \tag{22}$$

To consider the length scale and microstructure effect of nanobeam, substitute Eq. (22) into nonlocal strain gradient constitutive equation described by Eq. (8), yields

$$\begin{aligned}\delta u_0 &: \left(1 - \lambda\frac{\partial^2}{\partial x^2}\right)\left(A_{11}\frac{\partial^2 u_0}{\partial x^2} - B_{11}\frac{\partial^3 w_0}{\partial x^3} + B_{11}^s\frac{\partial^2 \phi_x}{\partial x^2}\right) = \left(1 - \mu\frac{\partial^2}{\partial x^2}\right)\left[I_0\ddot{u}_0 - I_1\frac{\partial \ddot{w}_0}{\partial x} + J_1\ddot{\phi}_x\right] \\ \delta w_0 &: \left(1 - \lambda\frac{\partial^2}{\partial x^2}\right)\left(B_{11}\frac{\partial^3 u_0}{\partial x^3} - D_{11}\frac{\partial^4 w_0}{\partial x^4} + D_{11}^s\frac{\partial^3 \phi_x}{\partial x^3}\right) + \left(1 - \mu\frac{\partial^2}{\partial x^2}\right)\left(q - N_x^0\frac{\partial^2 w_0}{\partial x^2}\right) \\ &= \left(1 - \mu\frac{\partial^2}{\partial x^2}\right)\left[-I_1\frac{\partial \ddot{u}_0}{\partial x} + I_0\ddot{w}_0 + I_2\frac{\partial^2 \ddot{w}_0}{\partial x^2} - J_2\frac{\partial \ddot{\phi}_x}{\partial x}\right] \\ \delta\phi_x &: \left(1 - \lambda\frac{\partial^2}{\partial x^2}\right)\left(B_{11}^s\frac{\partial^2 u_0}{\partial x^2} - D_{11}^s\frac{\partial^3 w_0}{\partial x^3} + H_{11}^s\frac{\partial^2 \phi_x}{\partial x^2} - A_{55}^s\phi_x\right) = \left(1 - \mu\frac{\partial^2}{\partial x^2}\right)\left[J_1\ddot{u}_0 - J_2\frac{\partial \ddot{w}_0}{\partial x} + K_2\ddot{\phi}_x\right]\end{aligned} \tag{23}$$

where the cross-sectional rigidities are expressed as

$$(A_{11}, B_{11}, D_{11}, B_{11}^s, D_{11}^s, H_{11}^s) = \int_{-h/2}^{h/2} Q_{11}(z)(1, z, z^2, f(z), z\,f(z), f(z)^2)dz \tag{24a}$$

$$A_{55}^s = \int_{-h/2}^{h/2} Q_{55}(z)g(z)^2 dz \tag{24b}$$

5. Analytical solution

The analytical solution of Eq. (23) can be solved using Galerkin approach for rectangular beams under various boundary conditions. The expressions of generalized displacements can be expressed a

$$\begin{Bmatrix} u_0 \\ w_0 \\ \phi_x \end{Bmatrix} = \sum_{m=1}^{\infty} \begin{Bmatrix} U_m \frac{\partial X_m}{\partial x} \\ W_m X_m \\ \Psi_{xm} \frac{\partial X_m}{\partial x} \end{Bmatrix} \tag{25}$$

with U_m, W_m and Ψ_{xm} being of the settings arbitrary. The functions $X_m(x)$ who satisfy the terms to boundaries selected are defined as

For beam SS

$$X_m = sin(\beta x)\,, \beta = \frac{m\pi}{L} \tag{26}$$

For beam CC

$$X_m = 1 - cos(\beta x)\,, \beta = \frac{2m\pi}{L} \tag{27}$$

For beam CS

$$X_m = [sin(\beta x)\, cos(\beta x) - 1], \beta = \frac{m\pi}{L} \tag{28}$$

Substituting equation (32) into equation (28), we get

$$[K_{ij}] \begin{Bmatrix} U_m \\ W_m \\ \psi_{xm} \end{Bmatrix} = 0, i, j = 1{:}3 \tag{29}$$

Where

$$\begin{gathered} K_{11} = A_{11}\left(\int_0^L \frac{\partial^3 X_m}{\partial x^3}\frac{\partial X_m}{\partial x}dx - \lambda\int_0^L \frac{\partial^5 X_m}{\partial x^5}\frac{\partial X_m}{\partial x}dx\right), K_{12} = -B_{11}\left(\int_0^L \frac{\partial^3 X_m}{\partial x^3}\frac{\partial X_m}{\partial x}dx - \right. \\ \left. \lambda\int_0^L \frac{\partial^5 X_m}{\partial x^5}\frac{\partial X_m}{\partial x}dx\right), K_{13} = B_{11}^S\left(\int_0^L \frac{\partial^3 X_m}{\partial x^3}\frac{\partial X_m}{\partial x}dx - \lambda\int_0^L \frac{\partial^5 X_m}{\partial x^5}\frac{\partial X_m}{\partial x}dx\right) \\ K_{21} = B_{11}\left(\int_0^L \frac{\partial^4 X_m}{\partial x^4}X_m\,dx - \lambda\int_0^L \frac{\partial^6 X_m}{\partial x^6}X_m\,dx\right) \\ K_{22} = -F_{11}\left(\int_0^L \frac{\partial^4 X_m}{\partial x^4}X_m\,dx - \lambda\int_0^L \frac{\partial^6 X_m}{\partial x^6}X_m\,dx\right) + \overline{N}_x^0\left(\int_0^L \frac{\partial^2 X_m}{\partial x^2}X_m\,dx - \right. \\ \left. \mu\int_0^L \frac{\partial^4 X_m}{\partial x^4}X_m\,dx\right)\ K_{23} = F_{11}^S\left(\int_0^L \frac{\partial^4 X_m}{\partial x^4}X_m\,dx - \lambda\int_0^L \frac{\partial^6 X_m}{\partial x^6}X_m\,dx\right) \\ K_{31} = B_{11}^S\left(\int_0^L \frac{\partial^3 X_m}{\partial x^3}\frac{\partial X_m}{\partial x}dx - \lambda\int_0^L \frac{\partial^5 X_m}{\partial x^5}\frac{\partial X_m}{\partial x}dx\right) \\ K_{32} = -F_{11}^S\left(\int_0^L \frac{\partial^3 X_m}{\partial x^3}\frac{\partial X_m}{\partial x}dx - \lambda\int_0^L \frac{\partial^5 X_m}{\partial x^5}\frac{\partial X_m}{\partial x}dx\right)\ K_{33} = H_{11}^S\left(\int_0^L \frac{\partial^3 X_m}{\partial x^3}\frac{\partial X_m}{\partial x}dx - \right. \\ \left. \lambda\int_0^L \frac{\partial^5 X_m}{\partial x^5}\frac{\partial X_m}{\partial x}dx\right) - K_{33}^S\left(\int_0^L \left(\frac{\partial X_m}{\partial x}\right)^2 dx - \lambda\int_0^L \frac{\partial^3 X_m}{\partial x^3}\frac{\partial X_m}{\partial x}dx\right) \end{gathered} \tag{30}$$

In the following section, the proposed theoretical solution is thoroughly examined to assess its accuracy. This evaluation is part of a comprehensive and systematic investigation that aims to determine the sensitivity of the buckling response. It is important to note that the proposed model

Table 1 Comparisons of dimensionless critical buckling load for S-S beam

V_{cnt}^{*}	L/h	Configuration of FG-CNTRC beam							
		UD		FG-X		FG-O		FG-V	
		Daikh *et al.* (2020b)	Present	Daikh *et al.* (2020b)	Present	Daikh *et al.* (2020b)	Present	Daikh *et al.* (2020b)	Present
0.12	10	0.1649	0.1649	0.2016	0.2016	0.1050	0.1050	0.2219	0.2222
	15	0.0986	0.0986	0.1294	0.1294	0.0574	0.0574	0.1450	0.1450
	20	0.0632	0.0632	0.0864	0.0864	0.0351	0.0351	0.0979	0.0980
0.17	10	0.2585	0.2585	0.3170	0.3170	0.1621	0.1621	0.3580	0.3581
	15	0.1504	0.1504	0.1985	0.1985	0.0862	0.0862	0.2263	0.2263
	20	0.0949	0.0949	0.1305	0.1305	0.0520	0.0520	0.1498	0.1498
0.28	10	0.3571	0.3571	0.4113	0.4113	0.2412	0.2412	0.4940	0.4940
	15	0.2201	0.2201	0.2763	0.2763	0.1323	0.1323	0.3282	0.3282
	20	0.1435	0.1435	0.1901	0.1901	0.0811	0.0811	0.2242	0.2242

is currently limited to uniform cross-sectional curved FG-CNTRC nanobeams. The analysis considers three types of boundary conditions: SS (simply supported), SC (simply clamped), and CC (clamped-clamped). Furthermore, the model assumes a linear variation of temperature across the thickness of the beam.

6. Results and discussion

This section demonstrates multiple numerical examples that assess the precision of a quasi-2D Higher-order Shear Deformation Theory (HSDT) in solving the buckling issue of FG-CNTRC straight beams. A comparison is made with existing solutions found in the literature. Additionally, we examine the influence of various parameters on the structural response of CNTRC sandwich beams. This investigation holds significant value for design considerations across various engineering applications. The numerical results are obtained for the beam made up of armchair (10,10) SWCNTs as reinforcement and Polymer matrix. The critical buckling load and the elastic foundation parameters are presented in the following non-dimensional form:

$$\overline{N}_{x0} = \frac{N_{x0}}{A_{110}}$$

where the coefficient A_{110} is of beam made of pure matrix material at room temperature T=300 K.

Initially, this study compares the numerical outcomes with previously conducted investigations. Subsequently, it examines the impact of geometric parameters on the dimensionless critical buckling load of the FG-CNTRC beam. Various scenarios involving different boundary conditions are considered during this analysis.

All the following studies are performed using poly methyl methacrylate (PMMA) as the matrix and its material properties are: $\upsilon^{P} = 0.3$, and $E^{P} = 2.5$ GPa. The (10,10) SWCNTs are selected as reinforcements whose properties are armchair (10,10) SWCNTs whose properties are: $\upsilon^{cnt} = 0.19$, $E_{11}^{cnt} = 600$ GPa, $E_{22}^{cnt} = 10$ GPa and $G_{12}^{cnt} = 17.2$ GPa.

According to Table 1, the dimensionless critical buckling load results of the FG-CNTRC beam obtained from the present two refined beam theory and the Galerkin solution align well with the

Table 2 Comparisons of dimensionless critical buckling load for C-C beam.

V_{cnt}^{*}	L/h	UD		FG-X		FG-O		FG-V	
		Daikh *et al.* (2020b)	present	Daikh *et al.* (2020b)	present	Daikh *et al.* (2020b)	present	Daikh *et al.* (2020b)	present
0.12	10	0.2850	0.2850	0.3154	0.3154	0.2113	0.2112	0.3422	0.3424
	15	0.2168	0.2168	0.2524	0.2524	0.1481	0.1481	0.2751	0.2752
	20	0.1649	0.1649	0.2016	0.2016	0.1050	0.1050	0.2219	0.2218
0.17	10	0.4663	0.4663	0.5114	0.5113	0.3468	0.3468	0.5729	0.5730
	15	0.3470	0.3470	0.4034	0.4034	0.2346	0.2346	0.4529	0.4529
	20	0.2585	0.2585	0.3170	0.3170	0.1621	0.1621	0.3580	0.3581
0.28	10	0.5913	0.5913	0.6127	0.6127	0.4817	0.4817	0.7488	0.7488
	15	0.4596	0.4596	0.5011	0.5011	0.3393	0.3393	0.6064	0.6065
	20	0.3571	0.3571	0.4113	0.4113	0.2412	0.2412	0.4940	0.4941

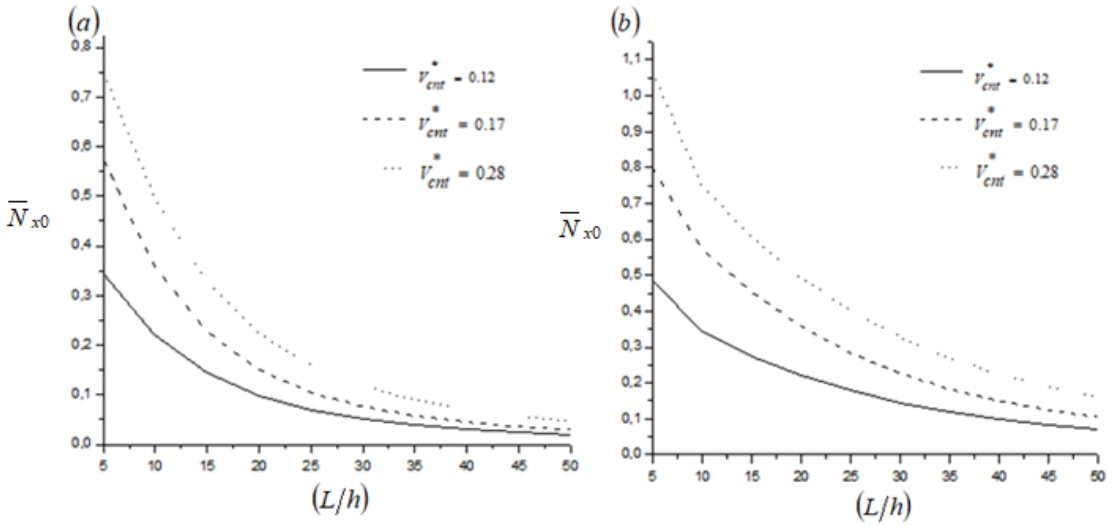

Fig. 2 Dimensionless critical buckling load of V-Beam with various thickness ratios (a) S-S beam and (b) C-C beam

buckling outcomes of high-order shear deformation theories presented by Daikh *et al.* (2020b).

This agreement indicates the reliability and consistency of the proposed methods in predicting the buckling behavior of the beam.

Table 2 present the dimensionless critical buckling load $\overline{N}_{x0}$ of FG-CNTRC clampled, using the four different CNT volume fractions and the different patterns of reinforcement, the results compared obtained with variation in the ratio of thickness L/h, it shows an improve in the dimensionless critical buckling load for all the different types of FG-CNTRC beams.

The highest loads are noticed at volume fraction $V_{cnt}^{*} = 0.28$, while the lowest values are for $V_{cnt}^{*} = 0.17$. The FG-V reinforcement patterns possess the peak critical buckling loads however, the smallest one is observed in the case of FG-O reinforcement patterns.

Fig. 2 exhibits the critical buckling load versus the thickness ratio (L/h)under various boundary conditions. The results obtained for simply supported conditions beam are smaller than

Table 3 Effect of nonlocal and length scale parameters on the critical buckling load of CNTRC beam ($L/h = 10, V_{cnt}^{*} = 0.12$)

μ	λ	S-S				C-C			
		UD	FG-X	FG-O	FG-V	UD	FG-X	FG-O	FG-V
0	0	0.1649	0.2016	0.1050	0.2222	0.2850	0.3154	0.2112	0.3424
	0.5	0.1730	0.2115	0.1101	0.2332	0.3412	0.3771	0.2530	0.4118
	1	0.1812	0.2215	0.1153	0.2442	0.3975	0.4400	0.2946	0.4809
	1.5	0.1893	0.2314	0.1205	0.2549	0.4537	0.5019	0.3364	0.5470
	2	0.1975	0.2414	0.1257	0.2661	0.5100	0.5640	0.3780	0.6152
0.5	0	0.1572	0.1921	0.1000	0.2116	0.2380	0.2633	0.1764	0.2872
	0.5	0.1649	0.2016	0.1050	0.2222	0.2850	0.3152	0.2112	0.3424
	1	0.1727	0.2111	0.1099	0.2324	0.3319	0.3672	0.2461	0.3995
	1.5	0.1804	0.2206	0.1148	0.2432	0.3789	0.4191	0.2811	0.4552
	2	0.1882	0.2301	0.1198	0.2536	0.4259	0.4714	0.3157	0.5125
1	0	0.1501	0.1835	0.0955	0.2021	0.2043	0.2260	0.1514	0.2449
	0.5	0.1575	0.1926	0.1002	0.2120	0.2446	0.2707	0.1814	0.2951
	1	0.1649	0.2016	0.1050	0.2222	0.2850	0.3152	0.2112	0.3424
	1.5	0.1723	0.2107	0.1097	0.2322	0.3253	0.3599	0.2412	0.3911
	2	0.1797	0.2197	0.1144	0.2421	0.3656	0.4045	0.2711	0.4409
1.5	0	0.1436	0.1756	0.0914	0.1936	0.1790	0.1981	0.1327	0.2151
	0.5	0.1507	0.1842	0.0959	0.2029	0.2143	0.2371	0.1588	0.2586
	1	0.1578	0.1929	0.1004	0.2127	0.2496	0.2764	0.1851	0.3009
	1.5	0.1649	0.2016	0.1050	0.2222	0.2850	0.3154	0.2112	0.3424
	2	0.1720	0.2103	0.1095	0.2318	0.3203	0.3544	0.2375	0.3860
2	0	0.1377	0.1684	0.0876	0.1856	0.1592	0.1760	0.1180	0.1913
	0.5	0.1445	0.1767	0.0920	0.1946	0.1906	0.2109	0.1413	0.2287
	1	0.1513	0.1850	0.0963	0.2037	0.2221	0.2458	0.1647	0.2673
	1.5	0.1581	0.1933	0.1006	0.2131	0.2535	0.2806	0.1879	0.3041
	2	0.1649	0.2016	0.1050	0.2222	0.2850	0.3152	0.2112	0.3424

that of the clamped-clamped beam. The highest loads are noticed at volume fraction $V_{cnt}^{*} = 0.28$, while the lowest values are for $V_{cnt}^{*} = 0.17$.

Tables 3, 4 and 5 depict the impact of nonlocal and length scale on the critical buckling loads of FG-CNTRC nanobeam using various boundary conditions. Clamped-Clamped nanobeams with FG-V distributions have the highest results.

It can be observed that buckling load increase by increasing of the length scale λ and by decreasing of the nonlocal parameter μ. On the other hand, the buckling load increases with increasing.

Fig. 3 illustrate the influence of the thickness ratio (L/h) of the simply supported nanobeam and clamped V-Beam for different values of nonlocal $\mu$and strain gradient parameters λ. It is clearly seen that when the nonlocal effect dominates $\mu > \lambda$, the dimensionless buckling loads is lower than those obtained by classical continuum theory $\mu = \lambda$, and the nanobeam is softened and becomes easy to deform. However, whenthe strain gradient effect dominates $\lambda > \mu$, the buckling is larger than those of classical continuum theory $\mu = \lambda$, and the nanobeam is hardened and becomes

Table 4 Effect of nonlocal and length scale parameters on the critical buckling load of CNTRC beam ($L/h = 10, V_{cnt}^{*} = 0.17$)

μ	λ	S-S				C-C			
		UD	FG-X	FG-O	FG-V	UD	FG-X	FG-O	FG-V
0	0	0.2585	0.3170	0.1621	0.3581	0.4663	0.5113	0.3468	0.5730
	0.5	0.2713	0.3327	0.1701	0.3758	0.5584	0.6123	0.4152	0.6863
	1	0.2841	0.3483	0.1781	0.3934	0.6505	0.7132	0.4836	0.8005
	1.5	0.2968	0.3640	0.1861	0.4111	0.7425	0.8141	0.5521	0.9131
	2	0.3096	0.3796	0.1941	0.4287	0.8346	0.9151	0.6206	1.0249
0.5	0	0.2464	0.3021	0.1545	0.3413	0.3895	0.4270	0.2896	0.4793
	0.5	0.2585	0.3170	0.1621	0.3581	0.4663	0.5113	0.3468	0.5730
	1	0.2707	0.3319	0.1697	0.3748	0.5432	0.5956	0.4039	0.6673
	1.5	0.2829	0.3469	0.1773	0.3917	0.6201	0.6799	0.4611	0.7616
	2	0.2950	0.3618	0.1849	0.4086	0.6970	0.7642	0.5183	0.8570
1	0	0.2353	0.2886	0.1475	0.3260	0.3343	0.3666	0.2486	0.4113
	0.5	0.2469	0.3028	0.1548	0.3419	0.4003	0.4390	0.2977	0.4920
	1	0.2585	0.3170	0.1621	0.3581	0.4663	0.5113	0.3468	0.5730
	1.5	0.2702	0.3313	0.1694	0.3742	0.5323	0.5837	0.3958	0.6537
	2	0.2818	0.3455	0.1766	0.3902	0.5984	0.6561	0.4449	0.7352
1.5	0	0.2252	0.2761	0.1412	0.3119	0.2929	0.3211	0.2178	0.3601
	0.5	0.2363	0.2898	0.1481	0.3272	0.3507	0.3845	0.2608	0.4309
	1	0.2474	0.3034	0.1551	0.3427	0.4085	0.4479	0.3038	0.5020
	1.5	0.2585	0.3170	0.1621	0.3581	0.4663	0.5113	0.3468	0.5730
	2	0.2697	0.3307	0.1690	0.3734	0.5242	0.5747	0.3898	0.6449
2	0	0.2159	0.2648	0.1354	0.2991	0.2606	0.2857	0.1937	0.3201
	0.5	0.2266	0.2778	0.1420	0.3138	0.3120	0.3421	0.2320	0.3835
	1	0.2372	0.2909	0.1487	0.3285	0.3635	0.3985	0.2703	0.4468
	1.5	0.2479	0.3040	0.1554	0.3433	0.4149	0.4549	0.3085	0.5100
	2	0.2585	0.3170	0.1621	0.3581	0.4663	0.5113	0.3468	0.5730

difficult to deform. In addition, with the increasing slenderness ratio, the dimensionless buckling load decreases when $\mu > \lambda$ and increases when $\lambda > \mu$, which is also counter to the situation of buckling response. Also, it can be seen that the differences between results predicted by classical theory and nonlocal strain gradient are significant for lower values of slenderness ratio but they are diminishing as the increase of slenderness ratio. Similar conclusions have also been observed about dynamic response based on the nonlo-cal strain gradient theory (Lu *et al.* 2017).

7. Conclusions

The size-dependent buckling analysis of symmetric and non symmetric carbon nanotube-reinforced composite (CNTRC) nanobeams with nonlocal strain gradient effects is investigated based on nonlocal strain gradient theory using a novel trigonometric shear deformation beams theory. The size effects are evaluated by introducing a nonlocal parameter and strain gradient

Table 5 Effect of nonlocal and length scale parameters on the critical buckling load of CNTRC beam ($L/h = 10, V_{cnt}^{*} = 0.28$)

μ	λ	S-S				C-C			
		UD	FG-X	FG-O	FG-V	UD	FG-X	FG-O	FG-V
0	0	0.3571	0.4113	0.2412	0.4940	0.5913	0.6127	0.4817	0.7488
	0.5	0.3747	0.4316	0.2531	0.5183	0.7080	0.7336	0.5768	0.8966
	1	0.3924	0.4519	0.2650	0.5428	0.8247	0.8546	0.6719	1.0445
	1.5	0.4100	0.4722	0.2769	0.5672	0.9415	0.9755	0.7670	1.1925
	2	0.4276	0.4925	0.2888	0.5915	1.0582	1.0965	0.8621	1.3399
0.5	0	0.3403	0.3920	0.2298	0.4707	0.4938	0.5117	0.4023	0.6248
	0.5	0.3571	0.4113	0.2412	0.4940	0.5913	0.6127	0.4817	0.7488
	1	0.3739	0.4307	0.2525	0.5172	0.6888	0.7137	0.5612	0.8724
	1.5	0.3907	0.4500	0.2639	0.5404	0.7863	0.8147	0.6406	0.9950
	2	0.4075	0.4694	0.2752	0.5637	0.8837	0.9157	0.7200	1.1193
1	0	0.3250	0.3744	0.2195	0.4497	0.4239	0.4393	0.3454	0.5364
	0.5	0.3411	0.3928	0.2303	0.4718	0.5076	0.5260	0.4136	0.6423
	1	0.3571	0.4113	0.2412	0.4940	0.5913	0.6127	0.4817	0.7488
	1.5	0.3732	0.4298	0.2520	0.5162	0.6750	0.6994	0.5499	0.8549
	2	0.3892	0.4483	0.2628	0.5383	0.7587	0.7861	0.6181	0.9608
1.5	0	0.3111	0.3583	0.2101	0.4303	0.3714	0.3848	0.3026	0.4703
	0.5	0.3264	0.3760	0.2204	0.4516	0.4447	0.4608	0.3623	0.5632
	1	0.3418	0.3936	0.2308	0.4727	0.5180	0.5367	0.4220	0.6554
	1.5	0.3571	0.4113	0.2412	0.4940	0.5913	0.6127	0.4817	0.7488
	2	0.3725	0.4290	0.2515	0.5152	0.6646	0.6886	0.5415	0.8412
2	0	0.2982	0.3435	0.2014	0.4125	0.3304	0.3423	0.2692	0.4184
	0.5	0.3130	0.3605	0.2113	0.4329	0.3956	0.4099	0.3223	0.5006
	1	0.3277	0.3774	0.2213	0.4533	0.4608	0.4775	0.3755	0.5836
	1.5	0.3424	0.3944	0.2312	0.4737	0.5261	0.5451	0.4286	0.6664
	2	0.3571	0.4113	0.2412	0.4940	0.5913	0.6127	0.4817	0.7488

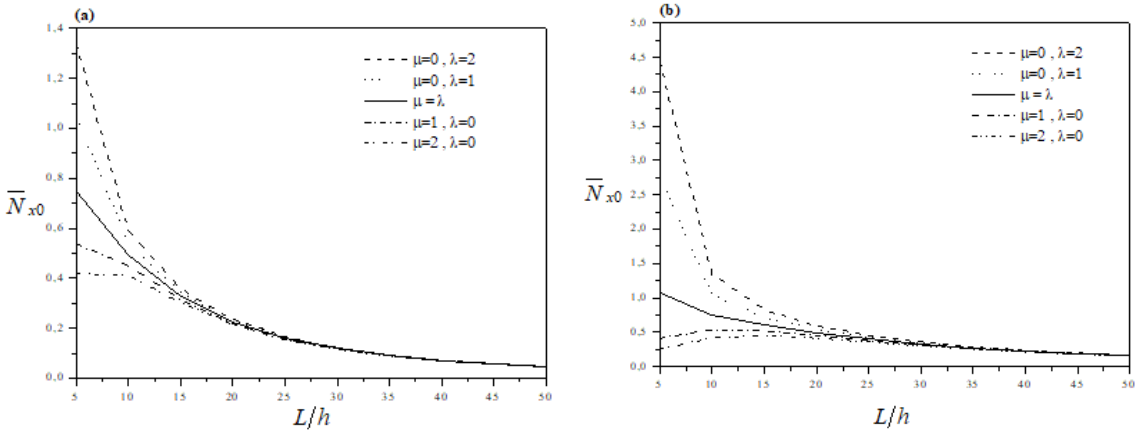

Fig. 3 Effect of nonlocal and length scale parameter on the dimensionless buckling load of V-Beam ($V_{cnt}^{*} = 0.28$): (a) simply supported beam, (b) clamped-clamped beam

parameter. The robustness and the reliability of the developed model are tested using analytical solutions. Galarkin's method is employed to get the analytical solutions for buckling responses of a simply supported and clamped nanobeam. A parametric study is conducted to bring out the influence of various parameters such as non-local parameter, strain gradient parameter and slenderness ratio considering different boundary conditions.

The following main points can be drawn from the present study:

1. The present formulation is in good agreement with those of analytical results and with those of the literature.
2. The response of the nanobeam depends largely on the nonlocal parameter, strain gradient parameter and slenderness ratio and it can be even qualitatively different.
3. With increasing the nonlocal parameter value, the dimensionless deflection value increases, the dimensionless critical buckling load and the frequency value decrease.
4. The nanobeam could exhibit either stiffness-softening effect or stiffness-hardening effect, which depends on the relative magnitude of the nonlocal parameter and the material length scale parameter.
5. The present novel theory is not only accurate but also simple in predicting the size-dependent buckling analysis of symmetric carbon nanotube-reinforced composite (CNTRC) nanobeams.

Finally, the formulation supports study into the behavior of isotropic, classical, and advanced composite macro/nanostructures, emphasizing the integration of stochastic methods and advanced computational techniques for accurate material modeling. Future research should extend these methodologies to diverse materials, refine computational efficiency, and validate models experimentally to enhance predictive capabilities in engineering applications (Nguyen *et al.* 2022, Ibrahimbegovic *et al.* 2022, Dobrilla *et al.* 2022, Tojaga *et al.* 2023, Dobrilla *et al.* 2023).

References

Alazwari, M.A., Daikh, A.A. and Eltaher, M.A. (2022a), "Novel quasi 3D theory for mechanical responses of FG-CNTs reinforced composite nanoplates", *Adv. Nano Res.*, **12**(2), 117. https://doi.org/10.12989/anr.2022.12.2.117.

Alazwari, M.A., Daikh, A.A., Houari, M.S.A., Tounsi, A. and Eltaher, M.A. (2021), "On static buckling of multilayered carbon nanotubes reinforced composite nanobeams supported on non-linear elastic foundations", *Steel Compos. Struct.*, **40**(3), 389-404. http://doi.org/10.12989/scs.2021.40.3.389.

Alazwari, M.A., Esen, I., Abdelrahman, A.A., Abdraboh, A.M. and Eltaher, M.A. (2022b), "Dynamic analysis of functionally graded (FG) nonlocal strain gradient nanobeams under thermo-magnetic fields and moving load", *Adv. Nano Res.*, **12**, 231-251. https://doi.org/10.12989/anr.2022.12.3.231.

Alibeigloo, A. (2014), "Free vibration analysis of functionally graded carbon nanotube-reinforced composite cylindrical panel embedded in piezoelectric layers by using theory of elasticity", *Eur. J. Mech.-A/Solid.*, **44**, 104-115. https://doi.org/10.1016/j.euromechsol.2013.10.002.

Bachiri, A., Daikh, A.A. and Tounsi, A. (2022), "On the thermo-elastic response of FG-CNTRC cross-ply laminated plates under temperature loading using a new HSDT", *J. Appl. Comput. Mech.*, **8**(4), 1370-1386. https://doi.org/10.22055/JACM.2022.40148.3529.

Belarbi, M.O., Houari, M.S.A., Hirane, H., Daikh, A.A. and Bordas, S.P.A. (2022), "On the finite element analysis of functionally graded sandwich curved beams via a new refined higher order shear deformation theory", *Compos. Struct.*, **279**, 114715. https://doi.org/10.1016/j.compstruct.2021.114715.

Bouafia, H., Chikh, A., Bousahla, A.A., Bourada, F., Heireche, H., Tounsi, A., ... & Hussain, M. (2021), "Natural frequencies of FGM nanoplates embedded in an elastic medium", *Adv. Nano Res.*, **11**(3), 239-249. https://doi.org/10.12989/anr.2021.11.3.239.

Chen, X., Zhao, J.L., She, G.L., Jing, Y., Pu, H. and Luo, J. (2021), "Nonlinear vibration analysis of functionally graded carbon nanotube reinforced fluid-conveying tube in thermal environment", *Steel Compos. Struct.*, **45**(5), 641. https://doi.org/10.12989/scs.2022.45.5.641.

Daikh, A.A., Bensaid, I., Bachiri, A., Houari, M.S.A., Tounsi, A. and Merzouki, T. (2020a), "On static bending of multilayered carbon nanotube-reinforced composite plates", *Comput. Concrete*, **26**(2), 137-150. http://doi.org/10.12989/cac.2020.26.2.137.

Daikh, A.A., Drai, A., Houari, M.S.A. and Eltaher, M.A. (2020b), "Static analysis of multilayer nonlocal strain gradient nanobeam reinforced by carbon nanotubes", *Steel Compos. Struct.*, **36**(6), 643-656. https://doi.org/10.12989/scs.2020.36.6.643.

Daikh, A.A., Houari, M.S.A., Belarbi, M.O., Mohamed, S.A. and Eltaher, M.A. (2022), "Static and dynamic stability responses of multilayer functionally graded carbon nanotubes reinforced composite nanoplates via quasi 3D nonlocal strain gradient theory", *Def. Technol.*, **18**(10), 1778-1809. https://doi.org/10.1016/j.dt.2021.09.011.

Daikh, A.A., Houari, M.S.A., Karami, B., Eltaher, M.A., Dimitri, R. and Tornabene, F. (2021), "Buckling analysis of CNTRC curved sandwich nanobeams in thermal environment", *Appl. Sci.*, **11**(7), 3250. https://doi.org/10.3390/app11073250.

De Borbón, F., Ambrosini, D. and Curadelli, O. (2014), "Damping response of composites beams with carbon nanotubes", *Compos. Part B: Eng.*, **60**, 106-110. https://doi.org/10.1016/j.compositesb.2013.12.041.

Dobrilla, S., Matthies, H.G. and Ibrahimbegovic, A. (2023), "Considerations on the identifiability of fracture and bond properties of reinforced concrete", *Int. J. Numer. Meth. Eng.*, **124**(17), 3662-3686. https://doi.org/10.1002/nme.7289.

Drai, A., Daikh, A.A., Belarbi, M.O., Houari, M.S.A., Aour, B., Hamdi, A. and Eltaher, M.A. (2023), "Bending of axially functionally graded carbon nanotubes reinforced composite nanobeams", *Adv. Nano Res.*, **14**(3), 211-224. https://doi.org/10.12989/anr.2023.14.3.211

Eringen, A.C. (1972), "Nonlocal polar elastic continua", *Int. J. Eng. Sci.*, **10**(1), 1-16. https://doi.org/10.1016/0020-7225(72)90070-5.

Eringen, A.C. (1983), "On differential equations of nonlocal elasticity and solutions of screw dislocation and surface waves", *J. Appl. Phys.*, **54**(9), 4703-4710. https://doi.org/10.1063/1.332803

Esmaeilzadeh, M., Esmaeil Golmakani, M., Kadkhodayan, M., Amoozgar, M. and Bodaghi, M. (2021), "Geometrically nonlinear thermo-mechanical analysis of graphene-reinforced moving polymer nanoplates", *Adv. Nano Res.*, **10**(2), 151-163. https://doi.org/10.12989/anr.2021.10.2.151.

Eyvazian, A., Zhang, C., Musharavati, F., Khan, A. and Mohamed, A.M. (2021), "Elastic wave phenomenon of nanobeams including thickness stretching effect", *Adv. Nano Res.*, **10**(3), 271. https://doi.org/10.12989/anr.2021.10.3.271.

Ghandourah, E.E., Ahmed, H.M., Eltaher, M.A., Attia, M.A. and Abdraboh, A.M. (2021), "Free vibration of porous FG nonlocal modified couple nanobeams via a modified porosity model", *Adv. Nano Res.*, **11**(4), 405. https://doi.org/10.12989/anr.2021.11.4.405.

Gholami, M., Azandariani, M.G., Ahmed, A.N. and Abdolmaleki, H. (2023), "Proposing a dynamic stiffness method for the free vibration of bi-directional functionally-graded Timoshenko nanobeams", *Adv. Nano Res.*, **14**(2), 127-139. https://doi.org/10.12989/.2023.14.2.127.

Gia Phi, B., Van Hieu, D., Sedighi, H.M. and Sofiyev, A.H. (2022), "Size-dependent nonlinear vibration of functionally graded composite micro-beams reinforced by carbon nanotubes with piezoelectric layers in thermal environments", *Acta Mechanica*, **233**(6), 2249-2270. https://doi.org/10.1007/s00707-022-03224-4.

Hajdo, E., Mejia-Nava, R.A., Imamovic, I. and Ibrahimbegovic, A. (2021), "Linearized instability analysis of frame structures under nonconservative loads: Static and dynamic approach", *Couple. Syst. Mech.*, **10**(1), 79-102. https://doi.org/10.12989/csm.2021.10.1.079.

Ibrahimbegovic, A. and Nava, R.A.M. (2021), "Heterogeneities and material-scales providing physically-based damping to replace Rayleigh damping for any structure size", *Couple. Syst. Mech.*, **10**(3), 201-216. https://doi.org/10.12989/csm.2021.10.3.201.

Ibrahimbegovic, A., Matthies, H.G., Dobrilla, S., Karavelić, E., Nava, R.A.M., Nguyen, C.U., ... &

Vondřejc, J. (2022), "Synergy of stochastics and inelasticity at multiple scales: novel Bayesian applications in stochastic upscaling and fracture size and scale effects", *SN Appl. Sci.*, **4**, 191. https://doi.org/10.1007/s42452-022-04935-y.

Ibrahimbegovic, A., Mejia-Nava, R.A., Hajdo, E. and Limnios, N. (2022), "Instability of (Heterogeneous) Euler beam: Deterministic vs. stochastic reduced model approach", *Couple. Syst. Mech*., **11**(2), 167-198. https://doi.org/10.12989/csm.2022.11.2.167.

Ibrahimbegovic, A., Rukavina, I. and Suljevic, S. (2022), "Multiscale model with embedded discontinuity discrete approximation capable of representing full set of 3D failure modes for heterogeneous materials with no scale separation", *Int. J. Multisc. Comput. Eng.*, **20**(1), 1-32. https://doi.org/10.1615/IntJMultCompEng.2021038378.

Iijima, S. (1991), "Helical microtubules of graphitic carbon", *Nature*, **354**(6348), 56-58.

Jin, Q., Yuan, F.G. and Ren, Y. (2022), "Resonance interaction of flow-conveying nanotubes under forced vibration", *Acta Mechanica*, 1-21. https://doi.org/10.1007/s00707-022-03425-x.

Ke, L.L., Yang, J. and Kitipornchai, S. (2013), "Dynamic stability of functionally graded carbon nanotube-reinforced composite beams", *Mech. Adv. Mater. Struct.*, **20**(1), 28-37. https://doi.org/10.1080/15376494.2011.581412.

Khadir, A. I., Daikh, A.A. and Eltaher, M.A. (2021), "Novel four-unknowns quasi 3D theory for bending, buckling and free vibration of functionally graded carbon nanotubes reinforced composite laminated nanoplates", *Adv. Nano Res.*, **11**(6), 621-640. https://doi.org/10.12989/anr.2021.11.6.621.

King, J.A., Via, M.D., Mills, O.P., Alpers, D.S., Sutherland, J.W. and Bogucki, G.R. (2012), "Effects of multiple carbon fillers on the electrical and thermal conductivity and tensile and flexural modulus of polycarbonate-based resins", *J. Compos. Mater.*, **46**(3), 331-350. https://doi.org/10.1177/0021998311422750.

Lim, C.W., Zhang, G. and Reddy, J. (2015), "A higher-order nonlocal elasticity and strain gradient theory and its applications in wave propagation", *J. Mech. Phys. Solid.*, **78**, 298-313. https://doi.org/10.1016/j.jmps.2015.02.001.

Lin, F. and Xiang, Y. (2014), "Vibration of carbon nanotube reinforced composite beams based on the first and third order beam theories", *Appl. Math. Model.*, **38**(15-16), 3741-3754. https://doi.org/10.1016/j.apm.2014.02.008.

Lu, L., Guo, X. and Zhao, J. (2017), "A unified nonlocal strain gradient model for nanobeams and the importance of higher order terms", *Int. J. Eng. Sci.*, **119**, 265-277. https://doi.org/10.1016/j.ijengsci.2017.06.024.

Moreno-Navarro, P., Ibrahimbegovic, A. and Damjanovic, D. (2021), "Multi-scale model for coupled piezoelectric-inelastic behavior", *Couple. Syst. Mech.*, **10**(6), 521-544. https://doi.org/10.12989/csm.2021.10.6.521.

Nguyen, C.U., Hoang, T.V., Hadzalic, E., Dobrilla, S., Matthies, H.G. and Ibrahimbegovic, A. (2022), "Viscoplasticity model stochastic parameter identification: Multi-scale approach and Bayesian inference", *Couple. Syst. Mech.*, **11**(5), 411-438. https://doi.org/10.12989/csm.2022.11.5.411

Okamoto, M. (2006), "Recent advances in polymer/layered silicate nanocomposites: An overview from science to technology", *Mater. Sci. Technol.*, **22**(7), 756-779. https://doi.org/10.1179/174328406X101319.

Rafiee, M., Yang, J. and Kitipornchai, S. (2013), "Large amplitude vibration of carbon nanotube reinforced functionally graded composite beams with piezoelectric layers", *Compos. Struct.*, **96**, 716-725. https://doi.org/10.1016/j.compstruct.2012.10.005.

Sagar, S., Iqbal, N., Maqsood, A., Shahid, M., Shah, N.A., Jamil, T. and Bassyouni, M.I. (2015), "Fabrication and thermal characteristics of functionalized carbon nanotubes impregnated polydimethylsiloxane nanocomposites", *J. Compos. Mater.*, **49**(8), 995-1006. https://doi.org/10.1177/0021998314528733.

Salem, K.S., Lubna, M.M., Rahman, A.M., NurNabi, M., Islam, R. and Khan, M.A. (2015), "The effect of multiwall carbon nanotube additions on the thermo-mechanical, electrical, and morphological properties of gelatin–polyvinyl alcohol blend nanocomposite", *J. Compos. Mater.*, **49**(11), 1379-1391.

https://doi.org/10.1177/0021998314534704.
Shen, H.S. (2009), "Nonlinear bending of functionally graded carbon nanotube-reinforced composite plates in thermal environments", *Compos. Struct.*, **91**(1), 9-19. https://doi.org/10.1016/j.compstruct.2009.04.026.
Shen, H.S. and Xiang, Y. (2012), "Nonlinear vibration of nanotube-reinforced composite cylindrical shells in thermal environments", *Comput. Meth. Appl. Mech. Eng.*, **213**, 196-205. https://doi.org/10.1016/j.cma.2011.11.025.
Shen, H.S. and Xiang, Y. (2013), "Nonlinear analysis of nanotube-reinforced composite beams resting on elastic foundations in thermal environments", *Eng. Struct.*, **56**, 698-708. https://doi.org/10.1016/j.engstruct.2013.06.002.
Suljevic, S., Ibrahimbegovic, A., Karavelic, E. and Dolarevic, S. (2022), "Meso-scale based parameter identification for 3D concrete plasticity model", *Couple. Syst. Mech.*, **11**(1), 55-78. https://doi.org/10.12989/csm.2022.11.1.055.
Tlidji, Y., Benferhat, R., Daouadji, T.H., Tounsi, A. and Trinh, L.C. (2022), "Free vibration analysis of FGP nanobeams with classical and non-classical boundary conditions using State-space approach", *Adv. Nano Res.*, **13**(5), 453-463. https://doi.org/10.12989/anr.2022.13.5.453.
Tojaga, V., Gasser, T.C., Kulachenko, A., Östlund, S. and Ibrahimbegovic, A. (2023), "Geometrically exact beam theory with embedded strong discontinuities for the modeling of failure in structures. Part I: Formulation and finite element implementation", *Comput. Meth. Appl. Mech. Eng*., **410**, 116013. https://doi.org/10.1016/j.cma.2023.116013.
Wattanasakulpong, N. and Ungbhakorn, V. (2013), "Analytical solutions for bending, buckling and vibration responses of carbon nanotube-reinforced composite beams resting on elastic foundation", *Comput. Mater. Sci.*, **71**, 201-208. https://doi.org/10.1016/j.commatsci.2013.01.028.
Witvrouw, A. and Mehta, A. (2005), "The use of functionally graded poly-SiGe layers for MEMS applications", *Mater. Sci. Forum*, **492**, 255-260. https://doi.org/10.4028/www.scientific.net/MSF.492-493.255.
Wu, H., Kitipornchai, S. and Yang, J. (2017), "Imperfection sensitivity of thermal post-buckling behaviour of functionally graded carbon nanotube-reinforced composite beams", *Appl. Math. Model.*, **42**, 735-752. https://doi.org/10.1016/j.apm.2016.10.045.
Yamamoto, N., de Villoria, R.G. and Wardle, B.L. (2012), "Electrical and thermal property enhancement of fiber-reinforced polymer laminate composites through controlled implementation of multi-walled carbon nanotubes", *Compos. Sci. Technol.*, **72**(16), 2009-2015. https://doi.org/10.1016/j.compscitech.2012.09.006.
Yas, M.H. and Samadi, N. (2012), "Free vibrations and buckling analysis of carbon nanotube-reinforced composite Timoshenko beams on elastic foundation", *Int. J. Press. Ves. Pip.*, **98**, 119-128. https://doi.org/10.1016/j.ijpvp.2012.07.012.
Zhao, J.L., Chen, X., She, G.L., Jing, Y., Bai, R.Q., Yi, J., ... & Luo, J. (2022), "Vibration characteristics of functionally graded carbon nanotube-reinforced composite double-beams in thermal environments", *Steel Compos. Struct*., **43**(6), 797-808. https://doi.org/10.12989/scs.2022.43.6.797.